Scilight

Environmental and Microbial Technology

https://www.sciltp.com/journals/emt

Review

Size Matters: A Comparison of Nanoparticle Catalysts vs. Single Atom Catalysts as Applied to Engineered Systems for Catalytic Oxidation Wastewater Sterilization

Fengting Geng [1] and Xing Xu [1,2,*]

[1] School of Environmental Science and Engineering, Shandong University, Qingdao 266237, China
[2] Shenzhen Research Institute of Shandong University, A301 Virtual University Park in South District of Shenzhen, Shenzhen 518057, China
* Correspondence: xuxing@sdu.edu.cn

How To Cite: Geng, F.; Xu, X. Size Matters: A Comparison of Nanoparticle Catalysts vs. Single Atom Catalysts as Applied to Engineered Systems for Catalytic Oxidation Wastewater Sterilization. *Environmental and Microbial Technology* **2026**, *1*(1), 9. https://doi.org/10.53941/emt.2026.100009

Received:13 January 2026
Revised: 29 January 2026
Accepted: 6 February 2026
Published: 26 February 2026

Abstract: Catalytic oxidation processes for engineering advanced wastewater sterilization have been well reported. Despite remarkable advancements, a systematic analysis of metal site dimensions (ranging from nanoscale clusters to single-atom configurations) for wastewater sterilization and their bactericidal properties/mechanisms remains conspicuously absent. This comprehensive review fills this critical void by rigorously examining how metallic site dimensionality governed reactive oxygen species (ROS) production in both photocatalytic and Fenton-like systems for water sterilization. The bactericidal efficacy of catalytic oxidation systems originates from size-mediated electronic configurations and geometric structures at metal active centers. Single-atom catalysts (SACs) achieve superior atomic efficiency in ROS production, while nanoparticle configurations demonstrate favorable cost-stability performance. These structural variations collectively determine microbe-catalyst contact dynamics, reactive oxygen formation, and material longevity under continuous operation, highlighting the necessity for tailored catalyst design strategies. We further culminate in highlighting enduring challenges including economic scalability and practical implementation barriers, while proposing innovative cross-disciplinary solutions incorporating machine learning (ML) methodologies. By establishing direct correlations between metal site architecture and bactericidal efficacy, this work seeks to inform the creation of advanced sustainable water purification technologies.

Keywords: catalytic oxidation; wastewater; sterilization; single-atom catalysts; nanoparticle

1. Introduction

The escalating global demand for clean water, coupled with the intensifying contamination of aquatic ecosystems by pathogenic microorganisms, underscores the critical need for advanced wastewater disinfection technologies [1–3]. Various conventional sterilization approaches, including chlorination, ultraviolet (UV) irradiation, and ozonation, remain widely adopted but suffer from inherent limitations [4–11]. Chlorination generates carcinogenic disinfection by-products (DBPs) [7,8], UV treatment exhibits poor penetration in turbid effluents [4–6], and ozonation requires high energy consumption and operational complexity [9–11]. With emerging antibiotic-resistant bacteria (ARBs) and persistent viral pathogens posing unprecedented public health risks, the development of robust, energy-efficient, and eco-friendly disinfection strategies has become a pressing priority. Effective sterilization not only safeguards water resources but also mitigates the transmission of

waterborne diseases, aligning with the United Nations Sustainable Development Goals for clean water and sanitation [12,13].

In contrast to traditional methods, catalytic oxidation processes have emerged as a transformative paradigm for pathogen inactivation, leveraging reactive oxygen species (ROS) such as hydroxyl radicals (•OH), superoxide anions ($•O_2^-$), and singlet oxygen ($^1O_2$) to disrupt microbial membranes and genetic materials [14–19]. Photocatalysis, exemplified by TiO_2-based systems, achieves broad-spectrum antimicrobial activity under solar irradiation but faces challenges in electron-hole recombination and limited visible-light utilization [20–23]. Fenton-like systems (e.g., Fe^{3+}/H_2O_2, metal oxides/peroxymonosulfate (PMS)) enable efficient ROS generation independent of light, yet pH dependency and metal leaching hinder scalability [24–26]. Recent advances integrate these systems into heterostructured or dual-functional catalysts, synergizing light absorption, charge separation, and radical cycling [27–38]. Crucially, catalytic oxidation processes minimize DBPs, operate at ambient conditions, and degrade organic pollutants concurrently, offering a sustainable solution for multifaceted water remediation.

The sterilization efficacy of catalytic oxidation processes is intrinsically linked to the atomic-scale architecture of catalytic metal sites, and their timeline was presented in Figure 1.

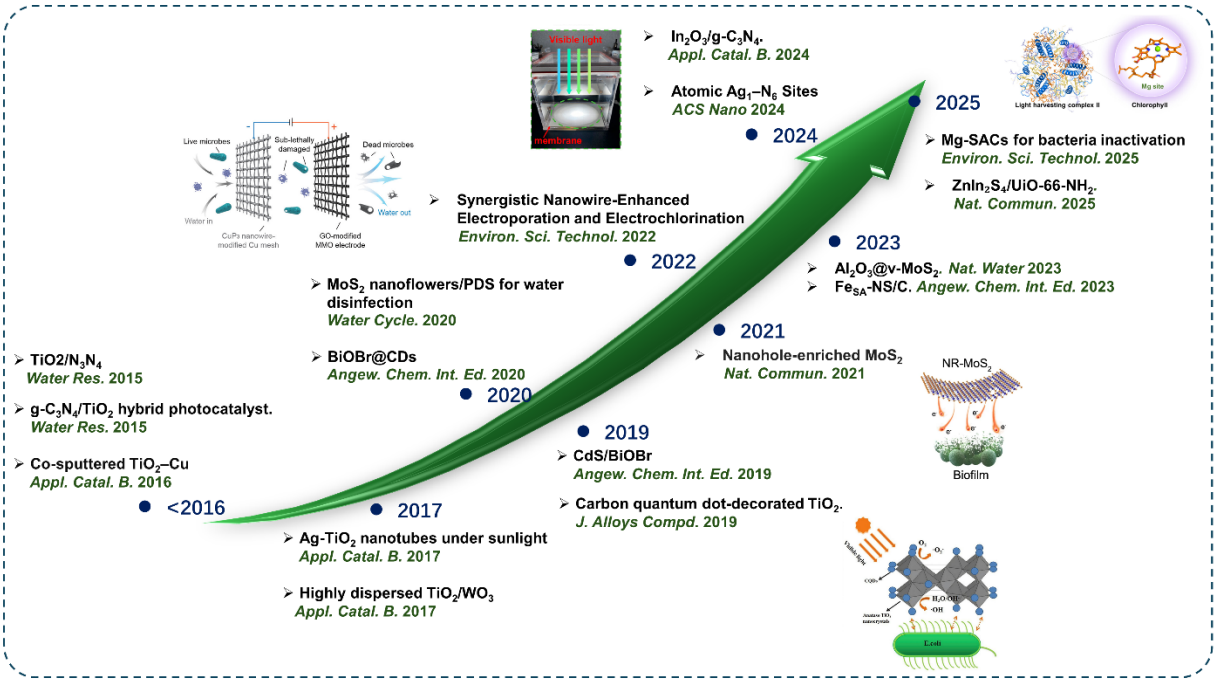

Figure 1. Timeline for the developments of catalytic oxidation processes based on versatile size-dependence catalysts for efficient water disinfection. Reproduced with permission [39]. Copyright 2019 Elsevier. Reproduced with permission [40]. Copyright 2022, American Chemical Society. Reproduced with permission [41]. Copyright 2024, American Chemical Society. Reproduced with permission [42]. Copyright 2025, American Chemical Society.

Early studies for the wastewater sterilization by the nano-based catalysts were mainly based on the TiO_2 and its derivatives [20–23]. For example, Li et al. assessed the visible-light-driven photocatalytic inactivation of Escherichia coli using g-C_3N_4/TiO_2 hybrid photocatalyst [21]. Rtimi et al. also reported the efficient photocatalytic bacterial inactivation capacity achieved by co-sputtered TiO_2–Cu [22]. Other photocatalysts such as Bi-series substances (BiOI, Bi_2O_3, BiOBr), nano-based Ag, as well as other metal semiconductors ZnO, SnO_2, WO_3 has been reported for the wastewater sterilization [43]. Recent breakthroughs in single-atom catalysts (SACs; e.g., Ag-SAC, Mn-N_4) redefine atomic efficiency [41,42,44], as isolated metal centers anchored on carbon or MOF substrates maximize ROS selectivity via optimized d-band electronic states. Concurrently, non-photocatalytic systems, such as piezocatalytic MoS_2 nanosheets or SACs-based Fenton-like systems [40,45–49], have expanded the operational scope of catalytic oxidation processes under diverse environmental conditions. Figure 2 compares the advantages and disadvantages of nano-based catalysts, SAC catalysts, and SAC and nano synergy catalyst. The study shows that compared to large-sized nanoparticles or bulk materials, SAC and SAC and nano synergy catalyst exhibit unique activity and reaction mechanisms. Moreover, the interaction between nanoparticles and SAC species also affects the activity, mechanism, and stability of catalytic oxidation [50]. This evolution reflects a paradigm shift toward precision engineering of metal sites to orchestrate ROS dynamics and interfacial interactions with pathogens.

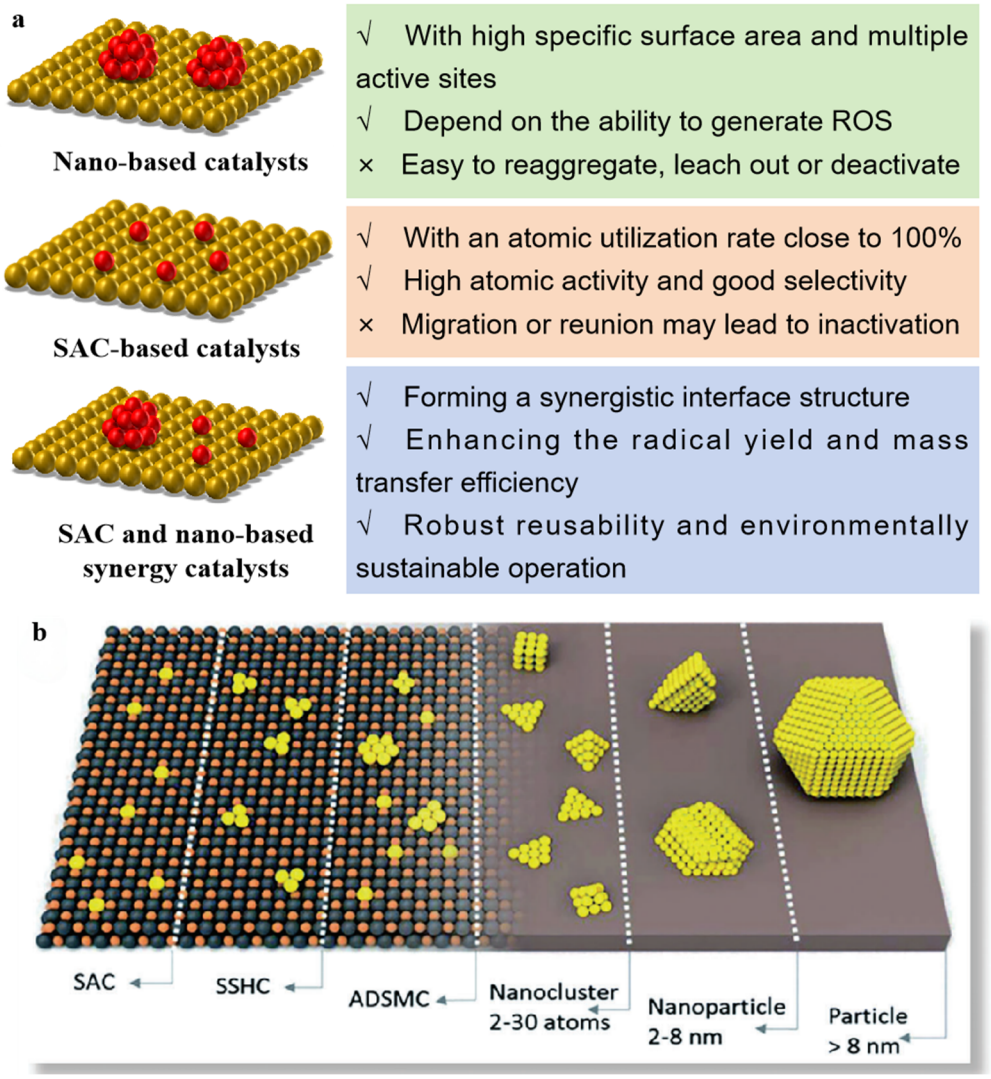

Figure 2. (**a**) Comparison of properties of Nano-based catalysts, SAC-based catalysts, and SAC and nano-based synergy catalysts. (**b**) Particle sizes for different metal-based catalysts. Reproduced with permission [50]. Copyright 2020, John Wiley and Sons.

Despite significant progress, a systematic analysis correlating metal site sizes (from the nanoscale to single atoms) with bactericidal mechanisms in catalytic oxidation processes remains lacking. Existing reviews primarily focus on material synthesis or ROS chemistry, often overlooking the size-dependent structure-activity relationships that govern pathogen-catalyst interactions. This review bridges the gap by critically evaluating how metal site size modulates ROS generation across photocatalysis and Fenton-like reactions for wastewater sterilization. We systematically review landmark studies to identify design principles for size-optimized catalysts, tracing the progression from empirical trial-and-error methods to atomically precise engineering. Furthermore, we identify persistent challenges, such as economic feasibility, scale-up application, and propose interdisciplinary strategies integrating machine learning. By elucidating the pivotal role of metal site dimensionality in catalytic disinfection, this work aims to inspire the development of next-generation, sustainable water sterilization technologies.

2. Nano-Based Catalysis for Wastewater Sterilization

Wastewater sterilization technology based on nano-metal catalytic sites achieves pathogen inactivation through the targeted generation of highly active species [51–55]. Photocatalytic oxidation (such as TiO_2 or Ag-based nanomaterials) utilizes photogenerated electron-hole pairs to produce ROS, which disrupt the microbial cell membrane and genetic material [56]. Fenton-like catalytic oxidation, on the other hand, relies on metal-based nanocatalysts to activate various oxidants (i.e., H_2O_2, PMS, peroxydisulfate (PDS)) and generate highly oxidative radicals or nonradicals, enabling rapid inactivation of drug-resistant pathogens [24–26]. Precise control of nanostructures (such as heterostructure construction or defect engineering) can further enhance catalytic activity, providing a new paradigm for the development of green and efficient wastewater disinfection technologies [57–60].

Light-driven catalysts are considered to be employed as effective strategies to solve environmental and energy problems owing to the green and safety property [61–68]. The H_2O_2 as well as various ROS, including •OH, $O_2^{\bullet-}$, $^1O_2$ and other active substances can be produced by light-triggered semiconductor materials to achieve the inactivation of bacteria owing to the satisfactory redox capability [16,54–56,61,62,69]. Membrane destruction, electron transport chain destruction, catalytic killing, cell division retardation and other antibacterial processes can be carried out by employing these ROS. For performing charming light-driven clean technology, the key factor in the design of semiconductors because ideal designed semiconductors can achieve more excellent light absorption, utilization and conversion, conducting the higher catalytic activity and light energy application [39,70].

TiO_2 has been extensively studied due to its excellent photocatalytic activity, low toxicity, and high chemical stability [2,71–73]. A typical photocatalytic bactericidal process of TiO_2 photocatalysts was given in Figure 3a, involving (i) bacterial oxidized by TiO_2 photocatalysis; (ii) bacterium leaked small molecules and ions, (iii) leakage of higher molecular weight components, (iv) degradation of bacterial internal components, and (v) mineralization of the bacterium [74]. TiO_2 exerts its bactericidal effect mainly through photocatalytic generation of ROS, with its performance governed by factors such as crystal structure, particle size, and surface defects [74]. However, its wide bandgap restricts light absorption primarily to the ultraviolet region, while rapid recombination of photogenerated electron–hole pairs and a typically negatively charged surface severely limit its practical efficacy [75,76]. Strategies including metal or non-metal doping, surface photosensitization, and hydrogenation treatment can effectively extend the optical absorption range, suppress charge carrier recombination, and thereby enhance visible-light responsiveness and dark-state antibacterial activity [74,77–79]. For example, carbon quantum dots (CQDs), leveraging their nanoscale dimensions and tunable surface functional groups, could generate ROS via photodynamic mechanisms or disrupt bacterial cell membranes through electrostatic interactions [39,80,81]. Consequently, CQDs/TiO_2 composite materials demonstrated remarkably improved antibacterial performance relative to pristine TiO_2 through the synergistic integration of three mechanisms: extended light absorption range, enhanced quantum efficiency, and reinforced bacterial targeting capability [39]. The three-phase "adsorption-destruction-oxidation" process ensured high efficiency, rapid kinetics, and comprehensive microbial inactivation [30,39,70]. These composites exhibit advantageous characteristics including broad-spectrum antimicrobial efficacy, visible-light responsiveness, sustained stability, and ecological compatibility, positioning them as promising candidates for advanced antibacterial applications.

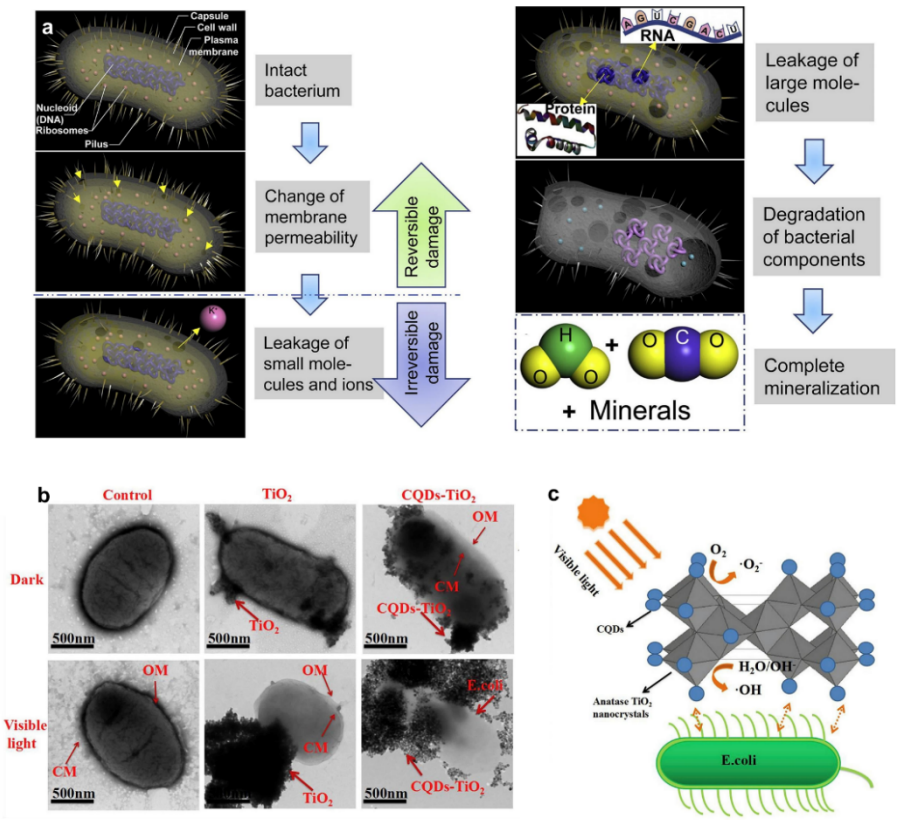

Figure 3. (**a**) Bactericidal procedure by the TiO_2-based photocatalysts. Reproduced with permission [74]. Copyright 2019 Elsevier. (**b**) TEM images of treated *E. coli* by TiO_2 and CQDs-TiO_2 composite. (**c**) Bactericidal mechanism of *E. coli* by CQDs-TiO_2 composite. Reproduced with permission [39]. Copyright 2019 Elsevier.

In addition to the TiO_2, numerous nano-photocatalysts (e.g., g-C_3N_4, metal sulfides, metal oxides such as ZnO and WO_3, two-dimensional materials) have emerged as research focal points in the field of wastewater disinfection due to their distinct performance advantages [27–38,82]. Graphitic carbon nitride (g-C_3N_4) exhibits excellent chemical stability and visible light responsiveness, enabling efficient charge separation through heterojunction engineering and facilitating disinfection via reactive species such as superoxide radicals and photogenerated holes [29,32,83]. Metal sulfides demonstrate strong visible light absorption and could generate potent hydroxyl radicals [34,35]; however, their limited stability necessitates structural modification or compositional hybridization to maintain catalytic activity. Metal oxides such as ZnO and WO_3 possess favorable band structures that allow concurrent generation of multiple ROS and holes [31,33], supporting simultaneous pollutant degradation and microbial inactivation. Bismuth-based materials offer high specific surface areas and enhanced visible light utilization, with surface modifications or composite formation further promoting radical generation for broad-spectrum antimicrobial action [25,84,85]. Two-dimensional materials, including transition metal sulfides and MXenes [29,36–38], leverage their layered architectures and superior electronic conductivity to accelerate charge transfer and enable targeted production of ROS, thereby achieving rapid and efficient disinfection under light irradiation. Collectively, these photocatalysts operate through photogenerated electron-hole pairs that induce the formation of hydroxyl radicals, •OH, $O_2^{\bullet-}$, and $^1O_2$, which effectively disrupt microbial cell membranes and intracellular components [27–38]. Their compatibilities with solar energy and environmentally benign nature make them promising candidates for sustainable, green wastewater treatment technologies. Future research could further prioritize in-depth investigation of interfacial charge transfer mechanisms using in-situ characterization techniques (e.g., XAFS), comprehensive biological safety evaluation, recyclability, and optimization of solar energy utilization under realistic and complex environmental conditions [70].

The catalytic system that rapidly generates the dominant $\bullet O_2^-$ through photocatalysis for water disinfection is an emerging green disinfection approach [57–60]. However, the spin-prohibited nature of molecular oxygen imposes limitations on the photocatalytic production of reactive $\bullet O_2^-$, consequently diminishing antimicrobial effectiveness under practical groundwater conditions characterized by insufficient dissolved oxygen levels [59,60]. Liu and co-workers recently engineered a class of torsionally modulated $Mo_{4/3}B_{2-x}T_z$MBene (MB) nanostructures exhibiting superior molecular oxygen adsorption/activation capabilities for photodynamic sterilization (Figure 4a,b) [57]. Experimental results revealed that lattice distortion-driven spin alignment in the $In_2S_3/Mo_{4/3}B_{2-x}T_z$ (IS/MB) heterostructure enabled optimized spin-orbital synergetic interactions between Mo active centers and O_2 molecules, effectively circumventing spin selection restrictions (Figure 4c). This innovation yielded an approximate 16.6-fold enhancement in photocatalytic $\bullet O_2^-$ generation under hypoxic aqueous conditions (Figure 4d). Notably, they further implemented a continuous-flow antimicrobial apparatus based on IS/MB, achieving prolonged operational stability (>62 h) with 37.2 L of microbially purified groundwater output, thereby establishing new benchmarks for photosterilization technologies (Figure 4e,f). Crucially, the system demonstrated 25-fold greater disinfection efficacy compared to conventional sodium hypochlorite (NaOCl) treatments, highlighting its transformative potential for practical water purification applications. Wu et al. achieved highly efficient heterogeneous photocatalytic disinfection through the construction of a (Al_2O_3@v-MoS_2)/Cu/Fe_3O_4 discrete nanostructure (Figure 4g,h) [58]. This novel composite integrated three key functional features (Figure 4i): (i) double-sided vertically aligned MoS_2 nanosheets grown on a transparent Al_2O_3 nanocarrier exhibited strong solar light absorption and enable simultaneous catalytic activity on both sides; (ii) the Cu–MoS_2 heterojunction significantly enhanced the separation and migration efficiency of photogenerated charge carriers, thereby promoting the effective generation of ROS; (iii) Fe_3O_4 magnetic nanoparticles allowed for rapid magnetic separation and straightforward post-treatment regeneration. Under natural sunlight irradiation, the resulting material could achieve complete inactivation of *E. coli* exceeding 5.7 log10 CFU/mL within 1 min, with minimal contribution from thermal effects. Furthermore, the (Al_2O_3@v-MoS_2)/Cu/Fe_3O_4 also demonstrated excellent cyclic stability, ease of recovery, and reliable reusability over multiple disinfection cycles.

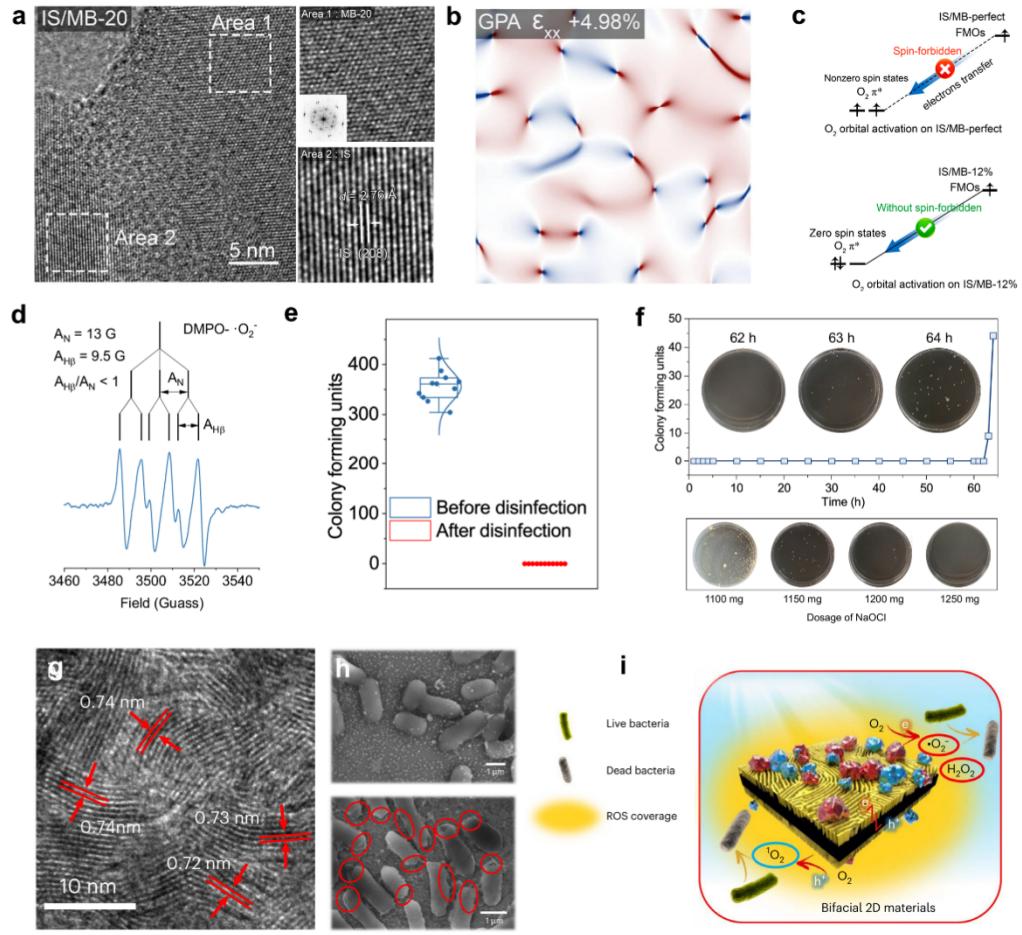

Figure 4. (**a**,**b**) TEM micrographs of the IS/MB composite with magnified views of regions 1–2, and their geometric phase analysis-derived lattice strain distribution. (**c**) Mechanism of spin-polarized transitions from IS/MB's frontier molecular orbitals to O_2 antibonding orbitals. (**d**) Operando EPR detection of photogenerated $•O_2^-$ in oxygen-deficient water. (**e**) Flow-through reactor's antimicrobial efficiency against groundwater microbial contaminants. (**f**) Comparative microbial culture visualization demonstrating bactericidal outcomes between IS/MB and NaOCl treatments. Reproduced with permission [57]. Copyright 2025 Nature. (**g**) TEM image revealing hierarchical architecture in Al_2O_3@v-MoS_2/Cu hybrid systems. (**h**) Comparative SEM micrographs illustrating low-speed centrifugal isolation efficacy for *E. coli* disinfection. (**i**) Solar-photon-driven ROS generation mechanism in ternary Al_2O_3@v-MoS_2/Cu/Fe_3O_4 photocatalytic assemblies. Reproduced with permission [58]. Copyright 2023 Nature.

In addition to the photocatalytic sterilization, a series of Fenton-like reactions with non-photocatalysis could also achieve the efficient sterilization process via activating various oxidants, such as PMS, PDS, H_2O_2 [24–26]. Li et al. found that BiOBr with oxygen vacancies (OVs) of appropriate density induced via ethanol reduction could effectively activate H_2O_2 (Figure 5a–d), achieving excellent ARB disinfection and antibiotic-resistant genes (ARGs) degradation efficiency [25]. Moreover, this disinfection system exhibited remarkable tolerance to complex water environments and actual water conditions. In-situ characterization and theoretical calculations revealed that OVs in BiOBr could effectively capture and activate aqueous H_2O_2 into •OH and $•O_2^-$. The generated ROS combined with electron transfer could damage the cell membrane system and degrade genetic materials of ARB (Figure 5e–g), leading to effective disinfection. Lu et al. reported that the MoS_2 nanoflowers deposited on porous graphite felt (MoS_2-GF) via the hydrothermal treatment could efficiently activate PDS for water disinfection (Figure 5h,i) [24]. MoS_2-activated PDS oxidation with 0.25 g/L MoS_2 and 0.2 mM PDS achieved above 7-log removal of *E. coli* within 25 min. $SO_4^{•-}$, •OH, and $•O_2^-$ were the main reactive radicals involved into bacteria inactivation. In addition, the live/dead backlight staining experiments and scanning electron microscopy characterization revealed that the bacteria were inactivated via cell membrane damage (Figure 5j,k). Despite these promising results, further efforts should address the management of residual oxidants to prevent secondary contamination, alongside advancing catalytic reactor designs (e.g., flow-through systems and immobilized catalyst configurations) to facilitate scalable implementation and cost-effective operation in diverse water treatment contexts.

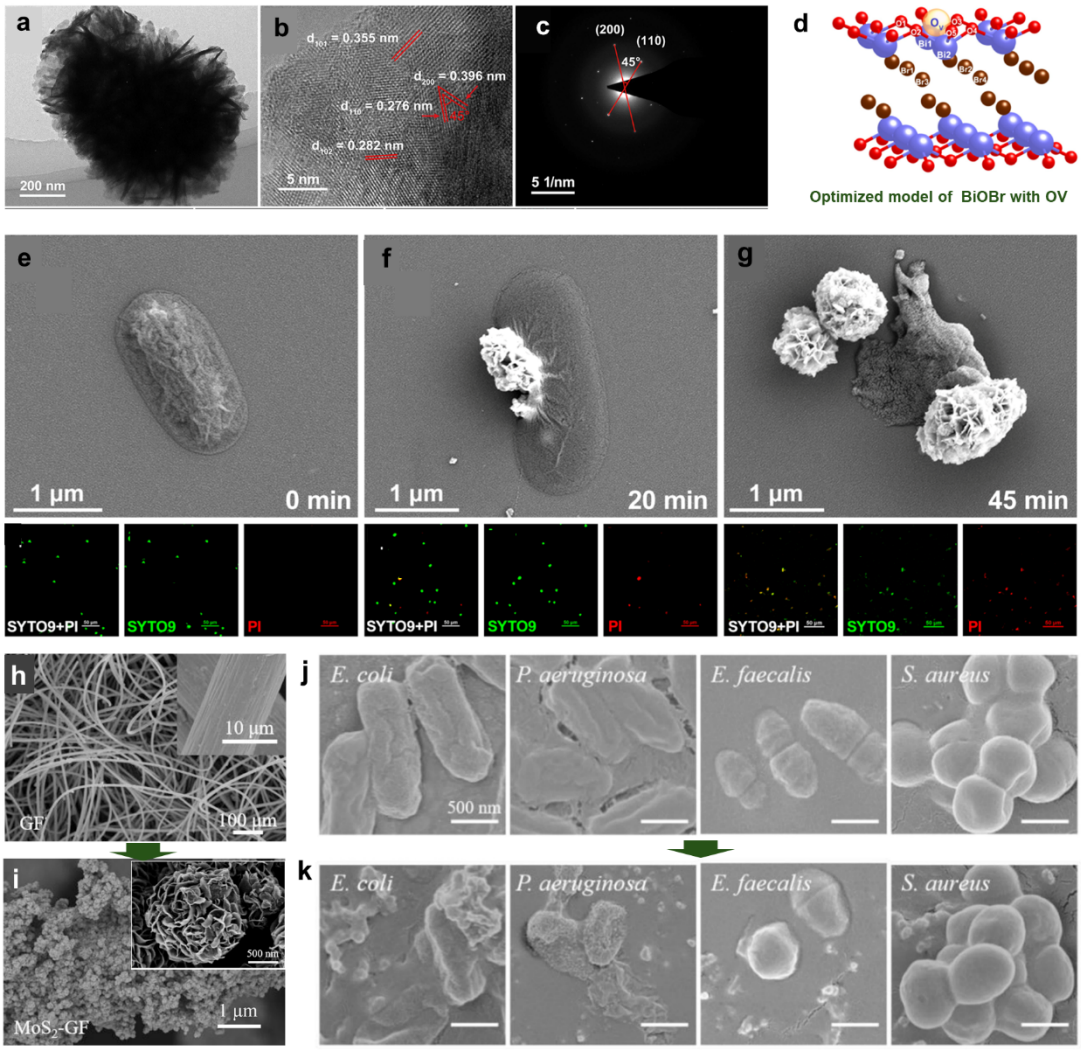

Figure 5. (**a**–**c**) TEM image and corresponding SEAD pattern of BiOBr with OV. (**d**) Optimized model of BiOBr with OV. (**e**–**g**) SEM image of *E. coli* at reaction of 0, 20, and 45 min. Reproduced with permission [25]. Copyright 2024, Elsevier Inc. (**h**,**i**) SEM images of pristine GF and MoS_2-GF. (**j**,**k**) SEM images of various pathogens before and after disinfection. Reproduced with permission [24]. Copyright 2022, Elsevier Inc.

3. SACs for Wastewater Sterilization

The SACs, with their maximized atomic utilization and well-defined active sites, are emerging as revolutionary platforms for photocatalytic sterilization systems [41,42,44,86–88]. Their atomic-level dispersion enables precise modulation of electronic structures, substantially enhancing ROS generation quantum efficiency while minimizing metal leaching risks [89–92]. Furthermore, the uniform single-site geometry permits targeted interactions with bacterial membranes and biomolecules, synergistically amplifying oxidative damage and resistance to biofilm formation [41,42,44,93].

Inspired by the natural light-harvesting mechanism of chlorophyll and the high catalytic efficiency of magnesium-containing coenzymes, Liu and colleagues rationally designed a catalytic system featuring atomically dispersed magnesium active sites embedded within ultrathin graphitic carbon nitride nanosheets (Figure 6a) [42]. The resulting catalyst demonstrated remarkable in situ bactericidal efficacy, achieving complete inactivation of *E. coli* within 80 min under visible light irradiation (Figure 6b). The highly dispersed magnesium single-atom sites enabled simultaneous activation of the water oxidation reaction and the two-electron oxygen reduction reaction (Figure 6c,d), thereby facilitating efficient in situ production of H_2O_2 through a dual-reaction pathway. Notably, when immobilized on a solid support, the catalyst maintained exceptional operational stability, sustaining a bactericidal efficiency exceeding 99.99% over 72 h of continuous operation, underscoring its potential for long-term antimicrobial applications (Figure 6e). Li et al. developed a template-free synthesis strategy to fabricate tubular g-C_3N_4 catalysts doped with high-loading zinc single atoms [44]. These atomically dispersed Zn active centers served as pivotal sites for promoting charge carrier separation and transfer, while simultaneously enhancing

surface O_2 adsorption affinity, thereby facilitating the efficient generation of $\bullet O_2^-$ for complete inactivation of *S. aureus*. Rao et al. developed silver single-atom-anchored g-C_3N_4 nanosheets (Ag_1/CN) and catalytic membranes for efficient inactivation of drug-resistant bacteria in multiple water bodies (Figure 6f). The incorporated Ag single atoms formed the Ag_1–N_6 coordination structures, which could significantly enhance the charge density around nitrogen atoms, thereby generating a strong built-in electric field. This electric field could effectively promote the charge separation efficiency of Ag_1/CN as well as lower the activation energy barrier for O_2 activation compared to the Ag NPs, enabling multi-ROS-mediated bacterial inactivation (Figure 6g,h). Moreover, the Ag_1/CN-based catalytic membrane maintained 99.9% bactericidal efficacy during continuous operation in a self-assembled flow reactor treating natural water and sewage, demonstrating excellent operational stability and promising potential for practical water disinfection applications (Figure 6i). These findings collectively demonstrated how precisely engineered single-atom architectures could drive next-generation photocatalytic sterilization technologies through enhanced ROS generation and optimized interfacial charge dynamics compared with the nano-based counterparts.

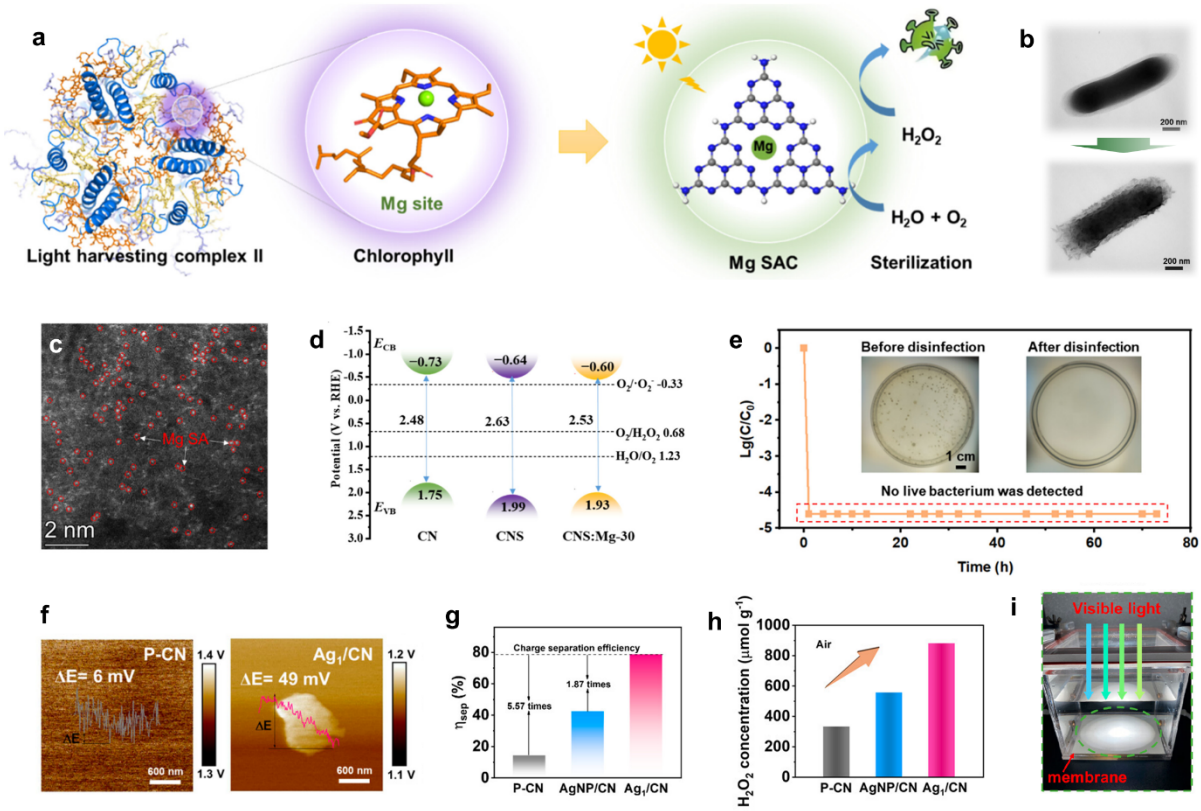

Figure 6. (**a**) Bioinspired Mg single-atom sites enabling photocatalytic H_2O_2 generation and on-site aqueous pathogen inactivation. (**b**) Comparative TEM visualization of *E. coli* morphology under dark conditions versus photocatalytic treatment. (**c**) Atomic-scale characterization of Mg single-atom configurations via HAADF-STEM. (**d**) Electronic band alignment illustration elucidating photocatalytic charge transfer mechanisms. (**e**) Operational durability of resulting catalyst in prolonged antimicrobial operation systems. Reproduced with permission [42]. Copyright 2025, American Chemical Society. (**f**) Surface potentials of bare P-CN and Ag_1/CN. (**g**) Charge separation rates of different catalysts. (**h**) H_2O_2 generation rate of different catalysts. (**i**) Photo of the visible-light Ag_1/CN/membrane system. Reproduced with permission [41]. Copyright 2024, American Chemical Society.

Recent advances in single-atom catalysis have also broadened the scope of aqueous microbial inactivation beyond conventional photodynamic strategies, as rationally engineered atomic architectures exhibit exceptional efficacy in activating a wide range of oxidants (i.e., PDS, PMS, H_2O_2), paralleling the performance of nanostructured catalysts [45–49]. Ma and colleagues developed a nitrogen-doped carbon-supported nickel-based single-atom catalyst (Ni–NC) featuring high-density Ni_2–N_6 dual-atomic sites, which enabled efficient generation of $^1O_2$ through synergistic PDS activation for effective sterilization (Figure 7a). Experimental results demonstrate that Ni–NC could markedly enhance the PDS activation capability compared to various nano-based catalysts and SACs, attributing to its optimal negative crystal orbital Hamiltonian population value (Figure 7b,c). The Ni_2–N_6 dual-atomic sites mediated the cooperative interaction between PDS and molecular oxygen (O_2), significantly

lowering the energy barrier of the rate-determining step and establishing an O_2-dependent dynamic disinfection enhancement mechanism. The resultant $^1O_2$ consequently inhibited horizontal gene transfer of antibiotic resistance through selective targeting of coenzyme Q biosynthesis, suppression of adenosine triphosphate (ATP) generation, and depolymerization of extracellular polymeric matrix components (Figure 7d). Wu et al. constructed a manganese single-atom nanozyme (EMSA-Mn-C_3N_4) system for periodate (PI) activation and systematically evaluated its bactericidal performance (Figure 7e) [49]. The EMSA-Mn-C_3N_4 nanozyme demonstrated superior biomimetic peroxidase-like catalytic activity compared to the Mn-NPs analogues and exhibited broad-spectrum antibacterial efficacy with effective biofilm proliferation inhibition within the PI system. Quantitative analysis based on the standard plate count method reveals that the inactivation efficiencies of methicillin-resistant *S. aureus* and *E. coli* reach 94.9% and 98.6%, respectively, confirming the practical applicability of the PI-AOPs system mediated by this nanozyme for water disinfection (Figure 7f,g). These findings establish a universal principle where strategically engineered single-atom centers can optimize ROS generation through multiple oxidative pathways compared with their nano-based counterparts, offering adaptable solutions for next-generation water disinfection technologies [41,45,94–96].

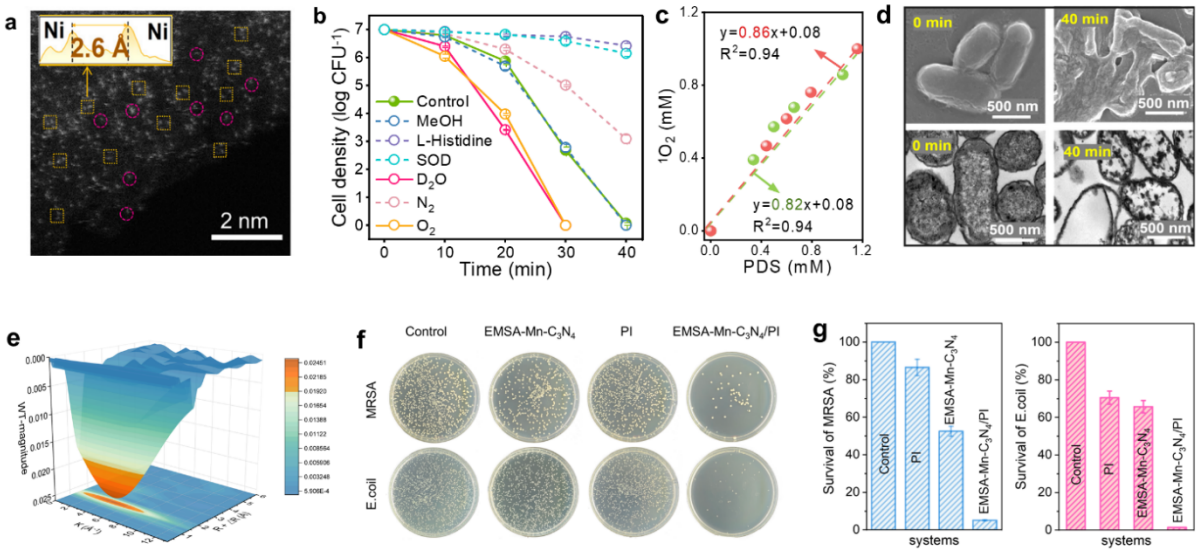

Figure 7. (**a**) HAADF-STEM images of the Ni–NC. (**b**) Effects of quenching agents on *E. coli* inactivation in the Ni–NC/PDS system. (**c**) Linear relationship between PDS consumption and $^1O_2$ production under air and O_2 conditions. (**d**) SEM and TEM images of *E. coli* collected during the inactivation process (0 and 40 min). Reproduced with permission [97]. Copyright 2025, American Chemical Society. (**e**) WT of EMSA-Mn-C_3N_4 nanozyme. (**f**) Quantitative analysis of inactivation efficiencies based on the standard plate count method. (**g**) Inactivation efficiencies of *S. aureus* and *E. coli* by different PI systems. Reproduced with permission [49]. Copyright 2025, Elsevier Inc.

Basically, the SACs demonstrate superior performance over conventional nanoparticle-based catalysts in wastewater sterilization by leveraging their atomic-level precision and maximized active site utilization. The atomically dispersed metal centers in SACs exhibit enhanced catalytic efficiency for ROS generation, enabling rapid and complete microbial inactivation through targeted oxidative damage to bacterial cell membranes, intracellular proteins, and genetic materials. Unlike nano-based catalysts, which often suffer from agglomeration-induced activity loss and pH-dependent metal leaching, SACs maintain structural stability and minimize secondary contamination risks. However, their practical implementation faces significant challenges. Specifically, (1). Due to the high surface energy of isolated metal atoms, they are prone to migration and agglomeration during synthesis and reaction, resulting in a reduction of active sites. (2). While increasing the metal loading (typically > 5 wt%), it is difficult to maintain atomic-level dispersion. The balance between high loading and high dispersion restricts the overall activity and efficiency of the catalyst. (3). The need to rely on extremely precise and sophisticated synthesis conditions and highly customized precursors leads to high energy consumption and material costs. (4). For different metal and carrier combinations, specific synthesis routes often need to be developed. Currently, there is still a lack of a universal, controllable, and efficient method for large-scale production [98,99]. Addressing these issues requires innovation in scalable fabrication techniques, durable carrier materials, and reactor designs that balance high-throughput sterilization with catalyst recovery. While SACs represent a transformative advancement

in precision water disinfection, bridging the gap between laboratory-scale success and industrial viability remains critical for their sustainable adoption.

4. Synergy of Single Atom and Nano-Sized Sites for Water Sterilization

Given the considerable technical barriers in engineering atomic-cluster catalytic systems, investigations into atomic-cluster sites that function as structural intermediaries bridging single atoms and nanoparticles for wastewater sterilization remain critically underexplored. However, the synergistic integration of single-atom sites and nano-sized counterparts has emerged as a revolutionary strategy for water sterilization [3,67,100]. This precisely engineered dual-active-center configuration combines atomic-level catalytic precision with plasmonic activation mechanisms, effectively addressing the inherent limitations of single-component systems in ROS generation and bacterial resistance elimination. A summary of catalytic oxidation for sterilization based on the size matters of catalysts was presented in Table 1.

Table 1. A summary of Catalytic Oxidation for sterilization Based on the Size Matters of Catalysts.

Size Matters	Catalysts	Activation Conditions	Reactive Species	Strains	Removal Efficiency	Ref.
Nano-based catalysts	CQDs-TiO_2	visible light	•OH	*E. coli* and *S. aureus*	90.9% and 92.8%, 1 d	[39]
	N,S-CQDs/Bi_2MoO_6@TiO_2	Visible light	•OH and $•O_2^-$	*E. coli*	100%, 1.5 h	[80]
	WO_{3-x}/MoS_2	Simulated solar	•OH, $•O_2^-$ and $^1O_2$	*E. coli* and *S. aureus*	94.23% and 93.09%, 20 min	[32]
	HJ-CN	Visible light	$•O_2^-$, H_2O_2 and h^+	MRSA	100%, 2 h	[83]
	Ru/WO_3/ZrO_2	Metal-halide lamp	•OH and h^+	gram-negative and gram-positive bacteria	90%, 2 h	[31]
	W/WO_3	UV-Vis light	•OH and $•O_2^-$	*C. parapsilosis*	100%, 5 min	[33]
	BOB-E	H_2O_2	•OH, $•O_2^-$ and charge transfer	*E. coli*	100%, 50 min	[25]
	MoS_2-GF	PDS	$SO_4^{•-}$, •OH, and $•O_2^-$	*E. coli*	above 7-log removal, 25 min	[24]
	CL_{HSO}	PMS	Electron transfer process	*E. coli*	100%, 30 min	[26]
SAC-based catalysts	ZCN	xenon lamp (300 W)	$•O_2^-$ and h^+	*S. aureus*	100%, 20 h	[40]
	CNS:Mg	300 W Xe arc lamp	$•O_2^-$	*E. coli*	99.99%, 80 min	[42]
	Ag_1/CN	visible-light	•OH and $•O_2^-$	*E. coli*, and *S. aureus*	99.9% and 99.9%, 4 h	[41]
	Fe SA/NPCs	PMS	$^1O_2$	*E. coli*	100%, 5 min	[45]
	EMSA-Mn-C_3N_4	PI	Electron transfer process	MRSA and *E. coli*	94.9% and 98.6%, -	[49]
SAC and nano synergy catalyst	CuPc-Dha-COF@AgNPs	near-infrared light	$•O_2^-$ and Ag^+	*E. coli*	100%, 10 min	[3]
	Ag_{SA+NP}/ZIF	Sunlight	$•O_2^-$ and H_2O_2	*E. coli*	99.99%, 30 min	[67]
	Pd_{AM-NP}/CNNT	visible-light	$•O_2^-$, $^1O_2$ and h^+	*E. coli*	100%, 5 h	[100]

Wang et al. constructed a novel floating monolithic photocatalyst system by co-loading silver single atoms (Ag_{SA}) and silver nanoparticles (Ag_{NP}) onto a monolithic ZIF-8-NH_2 carrier (denoted as Ag_{SA+NP}/ZIF), possessing both highly efficient sterilization and convenient recovery characteristics (Figure 8a–d) [67]. The sterilization efficiency of this composite material was over 2–3 orders of magnitude than those of Ag_{SA}/ZIF and Ag_{NP}/ZIF counterparts with superior stability (Figure 8e). The mechanism of superior action lied in that atomically dispersed Ag_{SA} could effectively promote the separation of photogenerated charges, thereby enhancing the generation of ROS such as H_2O_2 and $O_2^{•-}$ with its population 33.6-fold compared with Ag_{SA}/ZIF (Figure 8g); while Ag_{NP} with plasmonic effect destroyed the bacterial stress resistance system through photothermal effect, thereby weakening the bacteria's resistance to these ROS with more genes expression in *E. coli* (Figure 8f). Liu et al. developed a heterojunction material featuring uniformly distributed Cu-N_4 single-atom sites and silver nanoparticles with controllable size by using a metal phthalocyanine-based covalent organic framework (COF) as the porous architecture (Figure 8h–j) [3]. By carefully optimizing the synthesis conditions, they found that this composite demonstrated superior bacterial inactivation efficiency by combining multiple antibacterial mechanisms (Figure 8k,l), including synergistic photothermal and photodynamic effects, in-situ generation of H_2O_2, and controlled release of Ag^+, offering a promising solution for advanced antimicrobial applications.

The synergistic integration of single-atom and nano-sized dual-active centers constitutes a versatile platform that concurrently meets the key engineering demands of water sterilization, such as ultrahigh antibacterial efficacy, robust reusability, and environmentally sustainable operation. This catalytic system demonstrates an extremely low risk of metal leaching during actual operation and no obvious ecotoxicological effects have been observed. Its overall environmental safety performance is outstanding [100]. By harnessing complementary mechanisms such as excessive ROS generation and photothermal-enhanced antimicrobial action, these hybrid systems could achieve microbial inactivation efficiencies 2–3 orders of magnitude higher than those of single-component analogues [3,67]. This design strategy exhibited exceptional adaptability across diverse metal types (e.g., Ag, Cu) and support architectures (e.g., MOFs, COFs), indicating broad potential for advanced water purification technologies [3,67]. Although systematic investigations into single-atom/nanocluster synergies for wastewater disinfection are still limited, accumulating evidence supports their intrinsic universality across various metallic compositions [3,67]. A comprehensive examination of this universality across material classes will enable the establishment of predictive design principles for next-generation antimicrobial catalysts, particularly in complex wastewater environments where multifunctional inactivation pathways are essential.

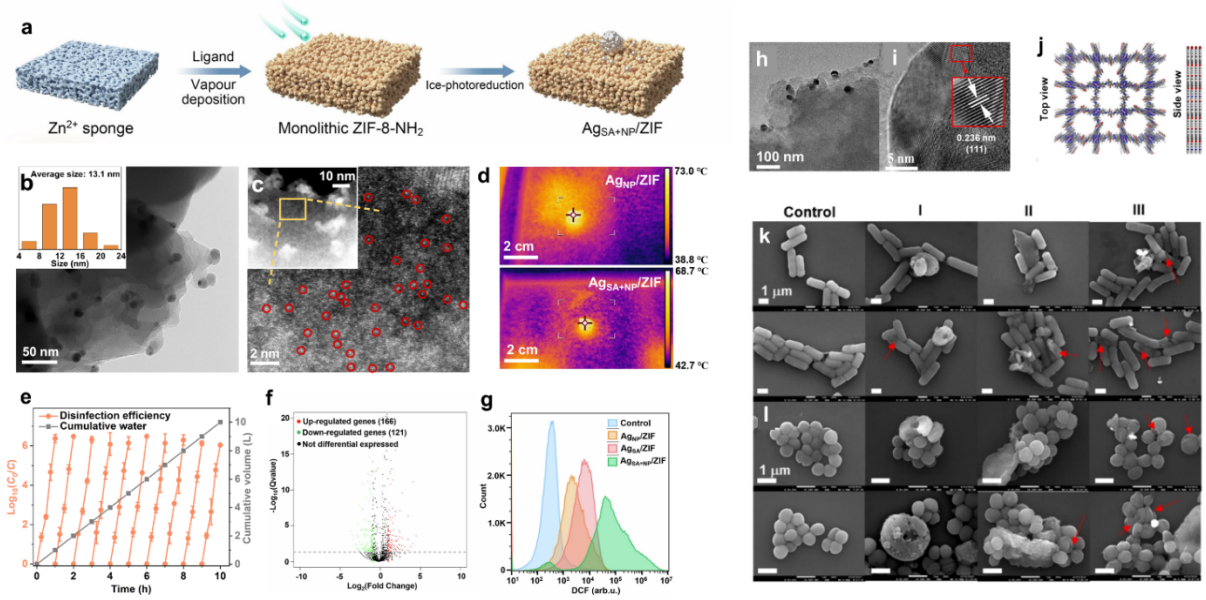

Figure 8. (**a**) Synthesis routine of the dual-active Ag_{SA+NP}/ZIF catalyst. (**b**,**c**) TEM image and AC-HAAD-STEM image of Ag_{SA+NP}/ZIF. (**d**) Aqueous heating profiles under ambient illumination following integrated photocatalyst introduction. (**e**) Disinfection stability of the Ag_{SA+NP}/ZIF catalyst. (**f**) ROS induction in *E. coli* under 15-min monolithic system exposure. (**g**) Transcriptomic volcano plot of Ag_{SA+NP}/ZIF-treated *E. coli* (15 min). Reproduced with permission [67]. Copyright 2025 Nature. (**h**,**i**) TEM and HR-TEM of CuPc-Dha-COF@AgNPs. (**j**) Top and side view of simulated structures of CuPc-Dha-COF. SEM images of (**k**) *E. coli* and (**l**) *S. aureus* after treated by different catalysts. Reproduced with permission [3]. Copyright 2024, Elsevier Inc.

5. Machine Learning (ML) Assisting

Machine learning (ML) is increasingly becoming a significant driving force for the intelligent development of catalytic oxidation sterilization technology, demonstrating remarkable advantages in catalyst design, process optimization, and antimicrobial substance screening, and gradually forming a closed-loop research model from molecular design to system optimization [101,102]. In the rational design of catalysts, ML can efficiently integrate multi-dimensional data such as catalyst structure, reaction conditions, and pollutant characteristics to construct a global optimization model. For instance, Gao et al. collected 652 sets of published experimental data and trained and compared four machine learning models including random forest (RF) (Figure 9a,b) [103]. The results indicated that the RF model performed the best, with the highest accuracy in predicting the catalytic oxidation rate constant (k). The prediction of k has a very high accuracy (test set) $R^2 = 0.82$. The model successfully identified key descriptors such as the number of d electrons of the central metal and the average electronegativity of the coordination environment, thereby guiding the synthesis of highly efficient catalysts with an optimal number of d electrons (5–7) and a lower electronegativity (<3.04). This approach transformed the traditional "trial and error" mode into an efficient "data-driven high-throughput screening and intelligent prediction", significantly shortening the research and development cycle of catalysts.

In terms of mechanism analysis and risk prediction of sterilization processes, the combination of ML and density functional theory (DFT) calculations can systematically predict the transformation pathways, intermediate products, and ecological risks of pathogenic microorganisms, pollutants, etc. during catalytic oxidation processes. Zhang and colleagues constructed a large reaction network containing 120 overall reactions and 9533 reaction steps in a visible light system mediated by S-doped TiO_2, and used machine learning to achieve rapid prediction of reaction Gibbs free energy change (ΔG) with accuracy close to DFT calculations [104]. At the same time, they proposed a multi-dimensional evaluation framework centered on "diversity ecotoxicity biodegradability feasibility" (DEBF), providing an operational path selection scheme between "efficiency" and "ecological safety", thereby achieving a shift from a process design that solely pursues efficiency to a "risk-aware" type that also considers ecological safety (Figure 9c).

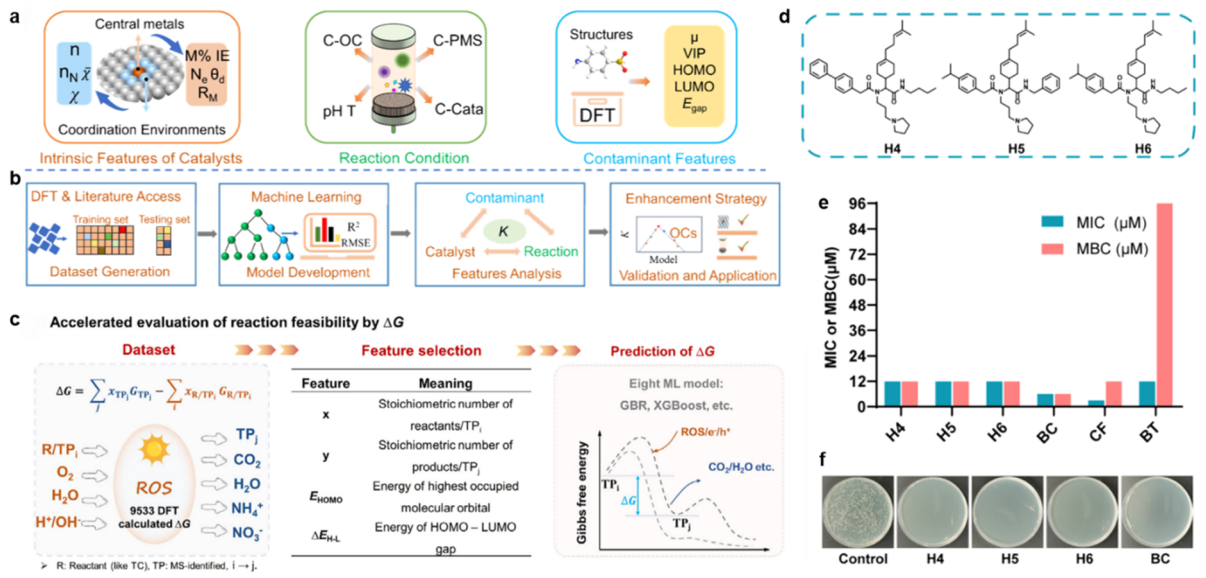

Figure 9. Global optimization strategy and model construction for SAC-driven catalytic oxidation. (**a**) Selection of the catalyst type, reaction conditions, and contaminant features. (**b**) workflow of the global optimization strategy. Reproduced with permission [103]. Copyright 2025, American Chemical Society. (**c**) Construction of the reaction database and extraction of molecular/reaction descriptors for ML model input. Reproduced with permission [104]. Copyright 2026, John Wiley and Sons. (**d**) Molecular structures of purified Ugi products H4–6. (**e**) MIC and MBC values of H4-6, CF and BT. (**f**) MRSA on TSA medium after 6 hours of incubation with H4–6 at 24 mM. Reproduced with permission [105]. Copyright 2024, Royal Society of Chemistry.

Furthermore, in the intelligent screening of highly efficient antibacterial substances, ML can rapidly identify high-activity antibacterial candidates from vast combinatorial chemistry libraries by integrating molecular fingerprints with physicochemical descriptors. To accurately predict the antibacterial activity of the entire compound library, Wang et al. developed a special spatially constrained neural network (LSCNN) model that combines molecular structure-activity relationship (SAR) and structure-property relationship (SPR) parameters [105]. After training the model with quantitative data from a relatively focused compound library, it can rank the antibacterial activity of the entire compound library. Validation experiments confirmed the activity of six hit compound combinations against methicillin-resistant Staphylococcus aureus (MRSA), demonstrating higher efficiency compared to blind screening of the entire compound library (Figure 9d–f). In summary, machine learning, through a data-driven approach, deeply integrates experiments and theoretical calculations, achieving full-chain optimization from catalyst design, reaction process control to product risk assessment, providing strong intelligent support for efficient and safe catalytic oxidation sterilization technology.

6. Conclusions and Perspective

The sterilization performance of catalytic oxidation systems is governed by the size-dependent electronic and geometric properties of metal active sites. SACs can maximize atomic utilization for promoting ROS generation, whereas nanoparticles provide cost-effective operational stability. These dimensional distinctions can also regulate pathogen–catalyst interaction mechanisms, ROS generation pathways, and long-term durability, underscoring the need for application-specific optimization.

Machine learning approaches are advancing the rational design of size-defined catalytic materials by enabling predictive simulations of optimal metal–support configurations, ROS activation mechanisms, and resistance to surface poisoning. Training datasets that integrate microbial inactivation kinetics, metal dispersion characteristics, and solvent effects facilitate efficient screening of single-atom catalysts for targeting antibiotic-resistant bacteria. Computational optimization methods improve synthesis protocols through precise control of pyrolysis conditions and ligand environments, thereby stabilizing isolated metal sites and suppressing nanoparticle aggregation. Real-time performance monitoring via machine learning in dynamic wastewater matrices allows adaptive operational adjustments and extends catalyst functional lifespan. The integration of computational catalysis, automated synthesis systems, and high-throughput characterization provides a robust framework for developing next-generation water purification technologies.

Future research should evaluate the economic feasibility of wastewater sterilization via metal site engineering, particularly the trade-off between the high activity of single-atom catalysts and their complex synthesis costs. Broadening the use of atom-dispersing strategies, such as spatial confinement and defect anchoring, can reduce precursor consumption. For nanoparticles, recycling protocols and alloy design can mitigate metal leaching and lower life-cycle expenses. A comprehensive techno-economic assessment that integrates material costs, energy input, and maintenance demands is essential for guiding practical implementation. Furthermore, reactor design must account for size-dependent reaction kinetics. Fixed-bed reactors loaded with nanoparticles can exploit their mechanical robustness in continuous-flow sterilization systems, whereas single-atom catalysts immobilized on porous membranes may enhance microbial inactivation efficiency in batch operations. Modular configurations should be adaptable to variations in catalyst dimensions and water matrix complexity. Ultimately, coupling catalytic units with pretreatment (e.g., filtration) or post-treatment (e.g., adsorption) modules can improve energy–water nexus efficiency.

Author Contributions

F.G.: Writing—original draft, Project administration, Formal analysis, Conceptualization. X.X.: Writing—review & editing, Visualization, Investigation, Funding acquisition.

Funding

The work was supported by National Natural Science Foundation of China (52170086), Natural Science Foundation of Shandong Province (ZR2021ME013) and Shandong Provincial Excellent Youth (ZR2022YQ47).

Data Availability Statement

Data will be made available on request.

Conflicts of Interest

The authors declare no conflict of interest.

Use of AI and AI-Assisted Technologies

No AI tools were utilized for this paper.

References

1. Li, J.; Chen, X.; Li, S.; et al. Construction of a flow-through catalytic reactor employing O_3–Fe/TiO_2 for efficient catalytic ozonation disinfection. *Catal. Sci. Technol.* **2024**, *14*, 6351–6362. https://doi.org/10.1039/d4cy00893f.
2. Yu, S.-Y.; Xie, Z.-H.; Wu, X.; et al. Review of advanced oxidation processes for treating hospital sewage to achieve decontamination and disinfection. *Chin. Chem. Lett.* **2024**, *35*, 108714. https://doi.org/10.1016/j.cclet.2023.108714.
3. Liu, J.; Guo, C.; Liu, Z.; et al. Simultaneous sterilization and biosensing of pathogenic bacteria via copper phthalocyanine-based COF embedded with Cu-N_4 single atomic sites and silver nanoparticles. *Chem. Eng. J.* **2024**, *494*, 153139. https://doi.org/10.1016/j.cej.2024.153139.
4. Zhou, C.-S.; Wu, J.-W.; Dong, L.-L.; et al. Removal of antibiotic resistant bacteria and antibiotic resistance genes in wastewater effluent by UV-activated persulfate. *J. Hazard. Mater.* **2020**, *388*, 122070. https://doi.org/10.1016/j.jhazmat.2020.122070.
5. Ping, Q.; Yan, T.; Wang, L.; et al. Insight into using a novel ultraviolet/peracetic acid combination disinfection process to simultaneously remove antibiotics and antibiotic resistance genes in wastewater: Mechanism and comparison with conventional processes. *Water Res.* **2022**, *210*, 118019. https://doi.org/10.1016/j.watres.2021.118019.

6. Meng, X.; Li, F.; Yi, L.; et al. Free radicals removing extracellular polymeric substances to enhance the degradation of intracellular antibiotic resistance genes in multi-resistant Pseudomonas Putida by UV/H_2O_2 and UV/peroxydisulfate disinfection processes. *J. Hazard. Mater.* **2022**, *430*, 128502. https://doi.org/10.1016/j.jhazmat.2022.128502.
7. Zhou, Y.; He, D.; Lei, Y.; et al. Bacterial inactivation by dichloride radical in water: Molecular-level reaction kinetics and disinfection mechanism. *Water Res.* **2026**, *288*, 124558. https://doi.org/10.1016/j.watres.2025.124558.
8. Aßmann, E.; Greiner, T.; Richard, H.; et al. Augmentation of wastewater-based epidemiology with machine learning to support global health surveillance. *Nat. Water* **2025**, *3*, 753–763. https://doi.org/10.1038/s44221-025-00444-5.
9. Azuma, T.; Usui, M.; Hayashi, T. Inactivation of antibiotic-resistant bacteria in hospital wastewater by ozone-based advanced water treatment processes. *Sci. Total Environ.* **2024**, *906*, 167432. https://doi.org/10.1016/j.scitotenv.2023.167432.
10. Wang, D.; Liu, Y.; Wang, Q.; et al. Activation of Peroxydisulfate via photothermal synergistic strategy for wastewater treatment: Efficiency and mechanism. *J. Hazard. Mater.* **2022**, *427*, 129224. https://doi.org/10.1016/j.jhazmat.2022.129224.
11. Jiang, L.; Li, J.; Kang, D.; et al. Unraveling Biological Ammonium Oxidation in Toxic Petrochemical Wastewater Treatment: A Metagenomic Exploration with Practical Implications. *ACS EST Eng.* **2025**, *5*, 2100–2107. https://doi.org/10.1021/acsestengg.5c00188.
12. Wang, W.-L.; Jing, Z.-B.; Zhang, Y.-L.; et al. Assessing the Chemical-Free Oxidation of Trace Organic Chemicals by VUV/UV as an Alternative to Conventional UV/H_2O_2. *Environ. Sci. Technol.* **2024**, *58*, 7113–7123. https://doi.org/10.1021/acs.est.3c08414.
13. Wang, Y.; Wu, Q.-Y.; Lee, M.-Y.; et al. Efficient Electrocatalytic Hydrodechlorination and Detoxification of Chlorophenols by Palladium–Palladium Oxide Heterostructure. *Environ. Sci. Technol.* **2024**, *58*, 20739–20750. https://doi.org/10.1021/acs.est.4c07923.
14. Kan, H.; Chou, X.; Li, M.; et al. Enhancing the chemoselective hydrogenation of o-chloronitrobenzene over nanoporous Ni/$NiAl_3$ catalysts. *Appl. Surf. Sci.* **2024**, *649*, 159120. https://doi.org/10.1016/j.apsusc.2023.159120.
15. Zhao, X.; Zhou, X.; Xia, Y.; et al. Realizing the high loading amount of active Cu on Al_2O_3 to boost its CO catalytic oxidation. *J. Colloid Interface Sci.* **2024**, *673*, 669–678. https://doi.org/10.1016/j.jcis.2024.06.130.
16. Pan, X.; Ji, J.; Zhang, N.; et al. Research progress of graphene-based nanomaterials for the environmental remediation. *Chin. Chem. Lett.* **2020**, *31*, 1462–1473. https://doi.org/10.1016/j.cclet.2019.10.002.
17. Jing, Z.-B.; Wang, W.-L.; Nong, Y.-J.; et al. Fluorescence analysis for water characterization: Measurement processes, influencing factors, and data analysis. *Water Reuse* **2022**, *13*, 33–50. https://doi.org/10.2166/wrd.2022.065.
18. Han, W.-R.; Wang, W.-L.; Qiao, T.-J.; et al. Ozone micro-bubble aeration using the ceramic ultrafiltration membrane with superior oxidation performance for 2,4-D elimination. *Water Res.* **2023**, *237*, 119952. https://doi.org/10.1016/j.watres.2023.119952.
19. Ouyang, W.-Y.; Wang, W.-L.; Zhang, Y.-L.; et al. VUV/UV oxidation performance for the elimination of recalcitrant aldehydes in water and its variation along the light-path. *Water Res.* **2023**, *228*, 119390. https://doi.org/10.1016/j.watres.2022.119390.
20. Xiao, G.; Zhang, X.; Zhang, W.; et al. Visible-light-mediated synergistic photocatalytic antimicrobial effects and mechanism of Ag-nanoparticles@chitosan–TiO_2 organic–inorganic composites for water disinfection. *Appl. Catal. B Environ.* **2015**, *170*, 255–262. https://doi.org/10.1016/j.apcatb.2015.01.042.
21. Li, G.; Nie, X.; Chen, J.; et al. Enhanced visible-light-driven photocatalytic inactivation of Escherichia coli using g-C_3N_4/TiO_2 hybrid photocatalyst synthesized using a hydrothermal-calcination approach. *Water Res.* **2015**, *86*, 17–24. https://doi.org/10.1016/j.watres.2015.05.053.
22. Rtimi, S.; Giannakis, S.; Sanjines, R.; et al. Insight on the photocatalytic bacterial inactivation by co-sputtered TiO_2–Cu in aerobic and anaerobic conditions. *Appl. Catal. B Environ.* **2016**, *182*, 277–285. https://doi.org/10.1016/j.apcatb.2015.09.041.
23. Mangayayam, M.; Kiwi, J.; Giannakis, S.; et al. FeO_x magnetization enhancing *E. coli* inactivation by orders of magnitude on Ag-TiO_2 nanotubes under sunlight. *Appl. Catal. B Environ.* **2017**, *202*, 438–445. https://doi.org/10.1016/j.apcatb.2016.09.064.
24. Lu, Y.-W.; Wang, C.; Joshi, N.; et al. MoS_2 nanoflowers-activated peroxydisulfate oxidation for rapid and efficient water disinfection. *Water Cycle* **2022**, *3*, 44–49. https://doi.org/10.1016/j.watcyc.2022.04.001.
25. Li, Z.; Hou, Y.; Shen, Y.; et al. Oxygen vacancy-dependent synergistic disinfection of antibiotic-resistant bacteria by BiOBr nanoflower induced H_2O_2 activation. *Water Res.* **2024**, *267*, 122524. https://doi.org/10.1016/j.watres.2024.122524.
26. Pei, W.; Hao, C.; Zhou, J.; et al. Peroxymonosulfate activation via non-contact electron transfer process (NCETP) for efficient organic pollutant removal. *Water Res.* **2026**, *289*, 124796. https://doi.org/10.1016/j.watres.2025.124796.
27. Ni, R.; Opoku, K.N.; Li, X.; et al. Recent advance in utilization of advanced composite photothermal materials for water disinfection: Synthesis, mechanism, and application. *Chin. Chem. Lett.* **2025**, *36*, 110813. https://doi.org/10.1016/j.cclet.2024.110813.
28. Li, X.; Wan, Y.; Deng, F.; et al. Advances in Z-scheme and S-scheme heterojunctions for photocatalytic and photoelectrocatalytic H_2O_2 production. *Chin. Chem. Lett.* **2025**, *36*, 111418. https://doi.org/10.1016/j.cclet.2025.111418.

29. Fang, Y.; Gao, H.; Cheng, K.; et al. An overview of photothermal materials for solar-driven interfacial evaporation. *Chin. Chem. Lett.* **2025**, *36*, 109925. https://doi.org/10.1016/j.cclet.2024.109925.
30. Ünsür, A.M.; Nejatpour, M.; Dükkancı, M.; et al. Green approach for perfluorocarboxylic acids (PFCAs) removal with density functional theory (DFT) insights: Peanut-shell biomass-based carbon quantum dots (PCQDs) coupled with TiO_2 photocatalyst. *J. Hazard. Mater.* **2025**, *495*, 139060. https://doi.org/10.1016/j.jhazmat.2025.139060.
31. Fouad, M.; Gar Alalm, M.; El-Etriby, H.K.; et al. Visible-light-driven photocatalytic disinfection of raw surface waters (300–5000 CFU/mL) using reusable coated $Ru/WO_3/ZrO_2$. *J. Hazard. Mater.* **2021**, *402*, 123514. https://doi.org/10.1016/j.jhazmat.2020.123514.
32. Mao, Q.; Wei, K.; Li, T.; et al. S-scheme WO_{3-x}/MoS_2 heterojunction photocatalysis coupling with micro-nano bubbles technology for enhanced antibacterial disinfection in water. *Environ. Res.* **2025**, *286*, 122966. https://doi.org/10.1016/j.envres.2025.122966.
33. Souza, B.A.; Giannini, M.J.S.M.; Yonashiro, M.; et al. Application of bioinspired W/WO_3 electrodes electrochemically constructed on microbial biofilm for the disinfection of dialysate contaminated by Candida parapsilosis. *J. Photochem. Photobiol.* **2023**, *16*, 100196. https://doi.org/10.1016/j.jpap.2023.100196.
34. Zhang, H.; Wang, Z.; Zhang, J.; et al. Metal-sulfide-based heterojunction photocatalysts: Principles, impact, applications, and in-situ characterization. *Chin. J. Catal.* **2023**, *49*, 42–67. https://doi.org/10.1016/S1872-2067(23)64444-4.
35. Aslam, A.; Nadeem, N.; Balgabayeva, B.; et al. Synergy in metal oxide/metal sulfide binary composites for photocatalysis: Mechanisms, applications, and emerging trends. *Inorg. Chem. Commun.* **2025**, *181*, 115191. https://doi.org/10.1016/j.inoche.2025.115191.
36. Liu, L.; Shen, Z.; Wang, C. Highly efficient visible-light-driven photocatalytic disinfection of flowing bioaerosol using mono/multilayer MXene based catalyst. *Chem. Eng. J.* **2023**, *457*, 141327. https://doi.org/10.1016/j.cej.2023.141327.
37. Bhattacharjee, B.; Ahmaruzzaman, M.; Djellabi, R.; et al. Advances in 2D MXenes-based materials for water purification and disinfection: Synthesis approaches and photocatalytic mechanistic pathways. *J. Environ. Manag.* **2022**, *324*, 116387. https://doi.org/10.1016/j.jenvman.2022.116387.
38. Li, J.; Yang, Z.; Wang, C.; et al. Rapid electron transfer via hetero-interface engineering of 2D MOF anchored Ti_3C_2 MXene nanosheet for enhanced photocatalytic disinfection. *Appl. Catal. B: Environ.* **2023**, *339*, 123163. https://doi.org/10.1016/j.apcatb.2023.123163.
39. Yan, Y.; Kuang, W.; Shi, L.; et al. Carbon quantum dot-decorated TiO_2 for fast and sustainable antibacterial properties under visible-light. *J. Alloys Compd.* **2019**, *777*, 234–243. https://doi.org/10.1016/j.jallcom.2018.10.191.
40. Huo, Z.-Y.; Winter, L.R.; Wang, X.-X.; et al. Synergistic Nanowire-Enhanced Electroporation and Electrochlorination for Highly Efficient Water Disinfection. *Environ. Sci. Technol.* **2022**, *56*, 10925–10934. https://doi.org/10.1021/acs.est.2c01793.
41. Rao, S.; Sun, Z.; Liu, Q.; et al. Engineering Atomic $Ag_1–N_6$ Sites with Enhanced Performance of Eradication Drug-Resistant Bacteria over Visible-Light-Driven Antibacterial Membrane. *ACS Nano* **2024**, *18*, 7074–7083. https://doi.org/10.1021/acsnano.3c10765.
42. Liu, L.-L.; Chen, F.; Wei, T.-T.; et al. Atomically Dispersed Magnesium Centers on Carbon Nitride for H_2O_2 Production and Synergistic in Situ Water Disinfection. *Environ. Sci. Technol.* **2025**, *59*, 21726–21737. https://doi.org/10.1021/acs.est.5c05354.
43. Gupta, R.; Boruah, B.; Modak, J.M.; et al. Kinet. Study Z-Scheme $C_3N_4/CuWO_4$ photocatalyst towards solar light inactivation of mixed populated bacteria. *J. Photochem. Photobiol. A: Chem.* **2019**, *372*, 108–121. https://doi.org/10.1016/j.jphotochem.2018.08.035.
44. Li, C.; Cai, Y.; Wu, J.; et al. High-concentration single-atom Zn-doped porous tubular g-C_3N_4: A superior photocatalyst for tetracycline hydrochloride degradation and bacterial sterilization. *Rare Met.* **2025**, *44*, 4756–4766. https://doi.org/10.1007/s12598-25-03279-x.
45. Yang, L.; Yang, H.; Yin, S.; et al. Fe Single-Atom Catalyst for Efficient and Rapid Fenton-Like Degradation of Organics and Disinfection against Bacteria. *Small* **2022**, *18*, 2104941. https://doi.org/10.1002/smll.202104941.
46. Tian, Q.; Xu, X.; Duan, X. Application-Oriented Advanced Oxidation Processes: Research Priorities for Upscaling and Deployment. *Environ. Sci. Technol.* **2025**, *59*, 16823–16826. https://doi.org/10.1021/acs.est.5c09384.
47. Tian, Q.; Chang, J.; Peng, X.; et al. Iron Single-Atom Based Double-Reaction-Center Catalysis Triggers Internal-Driven and External-Driven Pathways for Green Fenton-Like Chemistry. *Angew. Chem. Int. Ed.* **2025**, *64*, e202503995. https://doi.org/10.1002/anie.202503995.
48. Tian, Q.; Jiang, Y.; Duan, X.; et al. Low-peroxide-consumption fenton-like systems: The future of advanced oxidation processes. *Water Res.* **2025**, *268*, 122621. https://doi.org/10.1016/j.watres.2024.122621.
49. Yan, M.; Sun, J.; Chen, Y.; et al. Artificial manganese nanozyme for nonradical activation of periodate toward pH-universal water decontamination. *Chem Catal.* **2025**, *5*, 101299. https://doi.org/10.1016/j.checat.2025.101299.
50. Wu, J.; Xiong, L.; Zhao, B.; et al. Densely Populated Single Atom Catalysts. *Small Methods* **2020**, *4*, 1900540. https://doi.org/10.1002/smtd.201900540.

51. Ma, X.; Xu, Z.; Zhang, L.; et al. Nano zero-valent iron-based fiber electrode for efficient electro-Fenton treatment of pharmaceutical wastewater: Mechanism of degradation and sterilization. *Chem. Eng. J.* **2023**, *475*, 146049. https://doi.org/10.1016/j.cej.2023.146049.
52. Dong, L.; Cui, S.; Sun, X.; et al. Copper sulfides (Cu_7S_4) nanowires with Ag anchored in N-doped carbon layers optimize interfacial charge transfer for rapid water sterilization. *J. Colloid Interface Sci.* **2024**, *654*, 1209–1219. https://doi.org/10.1016/j.jcis.2023.10.140.
53. Zhang, X.; Yang, Z.; Zhang, J.; et al. Piezotronic effect enhanced catalytic sterilization: Mechanisms and practical applications. *Nano Energy* **2024**, *131*, 110346. https://doi.org/10.1016/j.nanoen.2024.110346.
54. Liu, J.; Huang, Y.; Song, X.; et al. Ni-Co synergistic regulation of catalyst surface charge density for efficient DNA base degradation in water. *J. Water Process Eng.* **2025**, *71*, 107313. https://doi.org/10.1016/j.jwpe.2025.107313.
55. Shen, Y.; Huang, J.; Qiao, J.; et al. Metal-based activation of periodate as an advanced oxidation process for water decontamination: A critical review. *Chem. Eng. J.* **2025**, *513*, 162949. https://doi.org/10.1016/j.cej.2025.162949.
56. Miao, J.; Geng, W.; Alvarez, P.J.J.; et al. 2D N-Doped Porous Carbon Derived from Polydopamine-Coated Graphitic Carbon Nitride for Efficient Nonradical Activation of Peroxymonosulfate. *Environ. Sci. Technol.* **2020**, *54*, 8473–8481. https://doi.org/10.1021/acs.est.0c03207.
57. Liu, Z.; Gao, W.; Liu, L.; et al. Spin polarization induced by atomic strain of MBene promotes the $\cdot O_2-$ production for groundwater disinfection. *Nat. Commun.* **2025**, *16*, 197. https://doi.org/10.1038/s41467-024-55626-8.
58. Wu, T.; Liu, B.; Liu, C.; et al. Solar-driven efficient heterogeneous subminute water disinfection nanosystem assembled with fingerprint MoS_2. *Nat. Water* **2023**, *1*, 462–470. https://doi.org/10.1038/s44221-023-00079-4.
59. Montemore, M.M.; van Spronsen, M.A.; Madix, R.J.; et al. O_2 Activation by Metal Surfaces: Implications for Bonding and Reactivity on Heterogeneous Catalysts. *Chem. Rev.* **2018**, *118*, 2816–2862. https://doi.org/10.1021/acs.chemrev.7b00217.
60. Peng, J.; Sokolov, S.; Hernangómez-Pérez, D.; et al. Atomically resolved single-molecule triplet quenching. *Science* **2021**, *373*, 452–456. https://doi.org/10.1126/science.abh1155.
61. Chen, S.; Ding, R.; Li, B.; et al. A robust aerogel incorporated with phthalocyanine-based porous organic polymers for highly efficient gold extraction. *Sep. Purif. Technol.* **2025**, *354*, 129451. https://doi.org/10.1016/j.seppur.2024.129451.
62. Wang, Q.; Li, F.; Yang, H.; et al. Simultaneous self-supply of H_2O_2 and GSH-depleted intracellular oxidative stress for enhanced photodynamic/photothermal/chemodynamic therapy. *Chem. Commun.* **2022**, *58*, 8536–8539. https://doi.org/10.1039/D2CC02961H.
63. Wang, C.; Zhao, X.; Hu, M.; et al. Unraveling Hydrocarbon Pool Boosted Propane Aromatization on Gallium/ZSM-5 Zeolite by Solid-State Nuclear Magnetic Resonance Spectroscopy. *Angew. Chem. Int. Ed.* **2021**, *60*, 23630–23634. https://doi.org/10.1002/anie.202111111.
64. Milenova, K.; Avramova, I.; Aleksieva, K. Investigation of $NiO/Pd/Al_2O_3$, $CuO/Pd/Al_2O_3$ and $CoO/Pd/Al_2O_3$ as catalysts for ozone decomposition and as photocatalysts. *Catal. Today* **2025**, *460*, 115439. https://doi.org/10.1016/j.cattod.2025.115439.
65. Lian, Z.; Gao, F.; Xiao, H.; et al. Photo-self-Fenton Reaction Mediated by Atomically Dispersed Ag−Co Photocatalysts toward Efficient Degradation of Organic Pollutants. *Angew. Chem. Int. Ed.* **2024**, *63*, e202318927. https://doi.org/10.1002/anie.202318927.
66. Luo, D.; Xiao, H.; Yang, Y.; et al. Photo-Self-Fenton Reaction Mediated by Silver Single Atom and Cluster Photocatalysts for Highly Selective Generation of Singlet Oxygen Toward Efficient Organic Wastewater Treatment. *Angew. Chem. Int. Ed.* **2025**, *64*, e202504028. https://doi.org/10.1002/anie.202504028.
67. Wang, J.; Zhang, J.; Li, Y.; et al. Silver single atoms and nanoparticles on floatable monolithic photocatalysts for synergistic solar water disinfection. *Nat. Commun.* **2025**, *16*, 981. https://doi.org/10.1038/s41467-025-56339-2.
68. He, F.; Lu, Y.; Jiang, G.; et al. Unveiling the dual charge modulation of built-in electric field in metal-free photocatalysts for efficient photo-Fenton-like reaction. *Appl. Catal. B Environ.* **2024**, *341*, 123307. https://doi.org/10.1016/j.apcatb.2023.123307.
69. Zhu, X.; Zong, H.; Pérez, C.J.V.; et al. Supercharged CO_2 Photothermal Catalytic Methanation: High Conversion. Rate, and Selectivity. *Angew. Chem. Int. Ed.* **2023**, *62*, e202218694. https://doi.org/10.1002/anie.202218694.
70. Cong, S.; Li, X.; You, J.; et al. Structural regulation and photocatalytic antibacterial performance of TiO_2, carbon dots and their nanocomposites: A review. *J. Colloid Interface Sci.* **2025**, *700*, 138482. https://doi.org/10.1016/j.jcis.2025.138482.
71. Jiang, X.; Hu, J.; Qin, Y.; et al. Novel dual bactericidal mechanism of TiO_2 'solution' during photocatalytic sterilization. *Appl. Surf. Sci.* **2025**, *688*, 162409. https://doi.org/10.1016/j.apsusc.2025.162409.
72. Rao, S.; Zhi, C.; Wang, X.; et al. In situ synthesis of graphitic carbon nitride nanosheet/$Ti_3C_2T_x$ MXene/TiO_2 Z-scheme heterojunctions boosting charge transfer for full-spectrum driven photocatalytic sterilization. *J. Colloid Interface Sci.* **2024**, *659*, 594–602. https://doi.org/10.1016/j.jcis.2024.01.005.
73. Wang, X.; Wang, J.; Liu, S.; et al. Sterilization mechanism and nanotoxicity of visible light-driven defective carbon nitride and UV-excited TiO_2. *J. Hazard. Mater.* **2024**, *461*, 132109. https://doi.org/10.1016/j.jhazmat.2023.132109.

74. Ge, X.; Ren, C.; Ding, Y.; et al. Micro/nano-structured TiO_2 surface with dual-functional antibacterial effects for biomedical applications. *Bioact. Mater.* **2019**, *4*, 346–357. https://doi.org/10.1016/j.bioactmat.2019.10.006.
75. Lee, J.H.; Kang, M.; Choung, S.-J.; et al. The preparation of TiO_2 nanometer photocatalyst film by a hydrothermal method and its sterilization performance for Giardia lamblia. *Water Res.* **2004**, *38*, 713–719. https://doi.org/10.1016/j.watres.2003.10.011.
76. Jung, H.; Kim, D.B.; Gweon, B.; et al. Enhanced inactivation of bacterial spores by atmospheric pressure plasma with catalyst TiO_2. *Appl. Catal. B Environ.* **2010**, *93*, 212–216. https://doi.org/10.1016/j.apcatb.2009.09.031.
77. Liu, Q.; Zhan, F.; Luo, H.; et al. Mechanism of interface engineering for ultrahigh piezo-photoelectric catalytic coupling effect of $BaTiO_3$@TiO_2 microflowers. *Appl. Catal. B Environ.* **2022**, *318*, 121817. https://doi.org/10.1016/j.apcatb.2022.121817.
78. Lu, Z.; Gao, J.; Rao, S.; et al. A multifunctional membrane based on TiO_2/PCN-224 heterojunction with synergistic photocatalytic-photothermal activity under visible-light irradiation. *Appl. Catal. B Environ.* **2024**, *342*, 123374. https://doi.org/10.1016/j.apcatb.2023.123374.
79. Jin, C.; Sun, D.; Sun, Z.; et al. Interfacial engineering of Ni-phytate and $Ti_3C_2T_x$ MXene-sensitized TiO_2 toward enhanced sterilization efficacy under 808 nm NIR light irradiation. *Appl. Catal. B Environ.* **2023**, *330*, 122613. https://doi.org/10.1016/j.apcatb.2023.122613.
80. Qu, Y.; Li, X.; Zhang, H.; et al. Controllable synthesis of a sponge-like Z-scheme N,S-CQDs/Bi_2MoO_6@TiO_2 film with enhanced photocatalytic and antimicrobial activity under visible/NIR light irradiation. *J. Hazard. Mater.* **2022**, *429*, 128310. https://doi.org/10.1016/j.jhazmat.2022.128310.
81. Rosales, S.; Medina, O.E.; Garzon, N.; et al. Systematic review of carbon quantum dots (CQD): Definition, synthesis, applications and perspectives. *Renew. Sustain. Energy Rev.* **2025**, *219*, 115854. https://doi.org/10.1016/j.rser.2025.115854.
82. Zhuang, C.; Chang, Y.; Li, W.; et al. Light-Induced Variation of Lithium Coordination Environment in g-C_3N_4 Nanosheet for Highly Efficient Oxygen Reduction Reactions. *ACS Nano* **2024**, *18*, 5206–5217. https://doi.org/10.1021/acsnano.4c00217.
83. Yang, X.; Sheng, L.; Ye, Y.; et al. Insights into the disinfection enhancement of homojunction g-C_3N_4 photocatalyst from charge transfer regulation and cell-surface attachment. *Chem. Eng. J.* **2023**, *474*, 145771. https://doi.org/10.1016/j.cej.2023.145771.
84. Kumar, R.; Raizada, P.; Verma, N.; et al. Recent advances on water disinfection using bismuth based modified photocatalysts: Strategies and challenges. *J. Clean. Prod.* **2021**, *297*, 126617. https://doi.org/10.1016/j.jclepro.2021.126617.
85. Ma, S.; Yu, X.; Li, W.; et al. Bismuth-based photocatalysts for pollutant degradation and bacterial disinfection in sewage system: Classification, modification and mechanism. *Environ. Res.* **2025**, *264*, 120297. https://doi.org/10.1016/j.envres.2024.120297.
86. Liu, J.; Goetjen, T.A.; Wang, Q.; et al. MOF-enabled confinement and related effects for chemical catalyst presentation and utilization. *Chem. Soc. Rev.* **2022**, *51*, 1045–1097. https://doi.org/10.1039/D1CS00968K.
87. Sharma, V.K.; Ma, X.; Zboril, R. Single atom catalyst-mediated generation of reactive species in water treatment. *Chem. Soc. Rev.* **2023**, *52*, 7673–7686. https://doi.org/10.1039/D3CS00627A.
88. Shang, Y.; Xu, X.; Gao, B.; et al. Single-atom catalysis in advanced oxidation processes for environmental remediation. *Chem. Soc. Rev.* **2021**, *50*, 5281–5322. https://doi.org/10.1039/D0CS01032D.
89. Li, R.; Zhao, J.; Liu, B.; et al. Atomic Distance Engineering in Metal Catalysts to Regulate Catalytic Performance. *Adv. Mater.* **2024**, *36*, 2308653. https://doi.org/10.1002/adma.202308653.
90. Ling, C.; Liu, X.; Li, H.; et al. Atomic-Layered Cu_5 Nanoclusters on FeS_2 with Dual Catalytic Sites for Efficient and Selective H_2O_2 Activation. *Angew. Chem. Int. Ed.* **2022**, *61*, e202200670. https://doi.org/10.1002/anie.202200670.
91. Ma, W.; Sun, M.; Huang, D.; et al. Catalytic Membrane with Copper Single-Atom Catalysts for Effective Hydrogen Peroxide Activation and Pollutant Destruction. *Environ. Sci. Technol.* **2022**, *56*, 8733–8745. https://doi.org/10.1021/acs.est.1c08937.
92. Xu, X.; Li, X.; Lu, W.; et al. Collective Effect in a Multicomponent Ensemble Combining Single Atoms and Nanoparticles for Efficient and Durable Oxygen Reduction. *Angew. Chem. Int. Ed.* **2024**, *63*, e202400765. https://doi.org/10.1002/anie.202400765.
93. Lu, H.; Li, X.; Li, F.; et al. Construction of single-atom Ag embedded O, K co-doped g-C_3N_4 with enhanced photocatalytic efficiency for tetracycline degradation and Escherichia coli disinfection under visible light. *J. Mol. Liq.* **2022**, *352*, 118655. https://doi.org/10.1016/j.molliq.2022.118655.
94. Li, F.; Liu, K.; Bao, Y.; et al. Molecular level removal of antibiotic resistant bacteria and genes: A review of interfacial chemical in advanced oxidation processes. *Water Res.* **2024**, *254*, 121373. https://doi.org/10.1016/j.watres.2024.121373.
95. Shi, T.; Hou, X.; Guo, S.; et al. Nanohole-boosted electron transport between nanomaterials and bacteria as a concept for nano–bio interactions. *Nat. Commun.* **2021**, *12*, 493. https://doi.org/10.1038/s41467-020-20547-9.
96. Wang, J.; Chu, L.; Wojnárovits, L.; et al. Occurrence and fate of antibiotics, antibiotic resistant genes (ARGs) and antibiotic resistant bacteria (ARB) in municipal wastewater treatment plant: An overview. *Sci. Total Environ.* **2020**, *744*, 140997. https://doi.org/10.1016/j.scitotenv.2020.140997.
97. Qi, W.; Tang, X.; Huang, Y.; et al. Electron Transfer Expressway from Peroxydisulfate to O_2 Mediated by Diatomic Sites Accelerating $^1O_2$ Production for Disinfection. *Environ. Sci. Technol.* **2025**, *59*, 15670–15679. https://doi.org/10.1021/acs.est.5c01975.

98. Zhang, H.; Duan, Y.; Elimelech, M.; et al. Scalable catalytic nanofiltration membranes for advanced water treatment. *Nat. Water* **2025**, *3*, 1038–1047. https://doi.org/10.1038/s44221-025-00483-y.
99. Yang, Y.; Li, H.; Fu, W.; et al. Large-scale deployment of single-atom catalysts via cross-scale confinement in ceramic membranes for advanced water treatment. *Nat. Water* **2025**, *3*, 1281–1290. https://doi.org/10.1038/s44221-025-00512-w.
100. Li, M.; Jiang, J.; Zhu, Z.; et al. Engineering Pd atom membrane-nanoparticle on carbon nitride for efficient photocatalytic water disinfection via in situ generation and activation of H_2O_2. *Chem. Eng. J.* **2025**, *509*, 161423. https://doi.org/10.1016/j.cej.2025.161423.
101. Duan, X.; Li, Y.; Zhao, J.; et al. Machine Learning Accelerated Discovery of Entropy-Stabilized Oxide Catalysts for Catalytic Oxidation. *J. Am. Chem. Soc.* **2025**, *147*, 651–661. https://doi.org/10.1021/jacs.4c12838.
102. Li, Q.; Xu, W.; Wang, W.; et al. Machine learning-driven screening and performance prediction of metal-organic frameworks for photocatalytic removal of malodorous methyl mercaptan. *J. Hazard. Mater. Adv.* **2025**, *19*, 100772. https://doi.org/10.1016/j.hazadv.2025.100772.
103. Gao, W.; Xu, Y.; Chang, X.; et al. Machine Learning-Driven Global Optimization of Single-Atom Catalyst-Mediated Advanced Oxidation Processes. *Environ. Sci. Technol.* **2025**, *59*, 24044–24054. https://doi.org/10.1021/acs.est.5c07237.
104. Zhao, C.-C.; Xing, S.; Fu, C.; et al. Mapping Antibiotic Photocatalytic Transformation and Resistance Risks with a DFT-Informed Machine Learning Workflow. *Angew. Chem. Int. Ed.* **2026**, e20124. https://doi.org/10.1002/anie.202520124.
105. Wang, C.; Wu, Y.; Xue, Y.; et al. Combinatorial discovery of antibacterials via a feature-fusion based machine learning workflow. *Chem. Sci.* **2024**, *15*, 6044–6052. https://doi.org/10.1039/D3SC06441G.